

Real-space understanding of electron-phonon coupling in superconducting hydrides

Trinidad Novoa,^{1,2,*} Raffaello Bianco,^{3,4} Julia Contreras-García,⁵ and Ion Errea^{1,2,6,†}

¹*Fisika Aplikatua Saila, Gipuzkoako Ingeniaritza Eskola,
University of the Basque Country (UPV/EHU),*

Europa Plaza 1, 20018 Donostia/San Sebastián, Spain

²*Centro de Física de Materiales (CSIC-UPV/EHU),*

Manuel de Lardizabal Pasealekua 5, 20018 Donostia/San Sebastián, Spain

³*Dipartimento di Scienze Fisiche, Informatiche e Matematiche,
Università degli Studi di Modena e Reggio Emilia, Modena, Italy*

⁴*Centro S3, Istituto Nanoscienze-CNR, Modena, Italy*

⁵*Laboratoire de Chimie Théorique, Sorbonne Université & CNRS, 4 Pl. Jussieu, 75005, Paris, France*

⁶*Donostia International Physics Center (DIPC),*

Manuel de Lardizabal Pasealekua 4, 20018 Donostia/San Sebastián, Spain

(Dated: July 10, 2025)

Electron-phonon coupling is at the origin of conventional superconductivity, enabling the pairing of electrons into Cooper pairs. The electron-phonon matrix elements depend on the electronic eigenstates and, in the standard linear approximation, on the first derivative of the potential felt by the electrons with respect to ionic perturbations. Here, we focus on the derivatives of the potential with a twofold aim: to assess their contribution to the overall coupling and to analyze the limitations of neglecting higher-order derivatives. Several real-space functions are proposed to do the analysis, and are computed for some well-known superconductors. Our results show that, in hydrides, the derivatives of the potential tend to be larger in regions of high electron localization, explaining the success of electronic descriptors previously described to correlate with the critical temperature. The new functions introduced here are able to tell apart structures with similar types of bonding but very different critical temperatures, such as H_3S and H_3Se $Im\bar{3}m$ phases, where electronic descriptors alone fail. Interestingly, our descriptors are capable of easily estimating the impact of higher-order terms in the electron-phonon coupling. In fact, we capture the limitations of the linear approximation expected for PdH, and predict an even more important non-linear behavior in LaH_{10} .

I. INTRODUCTION

Over the last century, scientists have been searching for superconductivity at ambient conditions. During this time, two very different families of superconductors have come closer to reaching room critical temperatures: cuprates and hydrogen-rich compounds. The former pose the great disadvantage of being unconventional, meaning that no theory accounts for superconductivity in those materials. Meanwhile, superconducting hydrides are stable only at megabar pressures [1–11], even if practically room temperature has been achieved for them. Nonetheless, they remain a topic of intense research given the prospects of discovering high-critical temperature (T_c) hydrides at low or even ambient pressures [12–24] and the conventional nature of their superconductivity, which allows the *ab initio* estimation of their T_c through the calculation of the electron-phonon interaction.

Theoretical estimations of T_c using the Migdal-

Eliashberg formalism require calculating the electronic wavefunctions and the first order derivatives of the effective electronic potential [25–27]. This, combined with the vastness of the chemical space of hydrides, makes theoretical prediction of new materials a cumbersome task. Using machine learning to accelerate the discovery of new superconductors is thus an attractive alternative, for which more than one approach has been adopted recently. On the one hand, it is possible to train the critical temperature directly from the chemical composition and structural information [28], or to add on top cheap electronic quantities like the density of states to improve the predictions of T_c [15, 29]. This kind of models allow to make very fast predictions, but training them is costly and requires extensive databases. Another approach is to train T_c using higher-level input quantities such as the Eliashberg function [30], which yields more accurate results but does not greatly reduce computation times with respect to standard first-principles calculations based on Migdal-Eliashberg theory. Finally, one can define cheap descriptors inspired by concepts used in quantum chemistry to characterize materials, and use them to train T_c [31, 32]. This option not only accelerates and improves the training, but it also provides physical insight into the properties that character-

* trinidadantonia.novoa@ehu.eus

† ion.errea@ehu.eus

ize high- T_c superconductors, as they contain more information on the electronic properties of the material, and describe the superconducting state [33]. In particular, in Refs. 31 and 32, electronic descriptors derived from the density of states (DOS) at the Fermi energy and from the electron localization function (ELF)[34, 35] were proposed. Both of them can be easily obtained in standard packages performing density functional theory (DFT) calculations, and the estimation of T_c can be obtained as a post-processing procedure that only takes a couple of seconds [36]. Nonetheless, those estimations are still far from accurate, which motivates the ongoing search for descriptors that could improve the characterization of hydride superconductors.

The ability of electronic properties to describe and predict superconductivity in conventional materials has been described in the literature several times[31, 32, 37–39]. However, because we are dealing with electron-phonon superconductors, we expect that the inclusion of vibrational properties should improve that description. In this context, the question arises as to whether the other part of the electron-phonon coupling – the one accounting for the changes of the ionic potential due to the vibrations – plays a significant role. Despite the previous observations suggesting that its role could be less important, a thorough study to confirm or deny that hypothesis is lacking. Moreover, because said correlations have only been proposed for hydrogen-based compounds, it is also in our interest to study the differences between conventional superconductors with and without hydrogen. We expect those differences to be important, owing to two very particular electronic and vibrational properties of hydrogen: that it does not have a core, and that the light weight of its nuclei can lead to large quantum ionic fluctuations.

In fact, in hydrides the phonon modes become highly anharmonic as a consequence of those quantum fluctuations, giving rise to non-negligible effects on the materials’ structural and dynamical properties [40–43]. The breakdown of the harmonic approximation is a reflection of the insufficiency of the second-order expansion of the Born-Oppenheimer (BO) potential to properly describe the ionic vibrations, which is a direct consequence of the large displacements of the hydrogen ions. In the case of the BO potential, a more adequate representation can be obtained by including higher-order derivatives in a non-perturbative way, for instance, within the stochastic self-consistent harmonic approximation (SSCHA) [44, 45]. The electron-phonon coupling is usually also calculated with a lowest-order linear expansion of the Kohn-Sham potential with respect to ionic displacements. However, considering the magnitude of the ionic displacements in hydrides, it seems contradictory to expect that only the linear part of the expansion should

be enough for the electron-phonon coupling, but that anharmonic effects in the BO potential need to be considered for the structural and dynamical properties.

Estimating the electron-phonon coupling beyond the linear approximation is very cumbersome and few materials have been studied thus far from first principles [46–52]. In Ref. 47, this was done for palladium hydride and aluminum, confirming that non-linear effects are significantly more pronounced in the superconductor containing hydrogen. For PdH, a linear approach led to large discrepancies in the electron-phonon coupling constant, which is crucial for estimating T_c . Little is known about similar behaviors in other hydrides, and the consequences that this could have on the estimation of electron-phonon coupling and critical temperature in those materials.

By including explicitly the analysis of the derivatives of the Kohn-Sham potential, in this paper we present new real-space functions and descriptors to predict T_c that improve previous ones in the literature only based on electronic properties. We also demonstrate how these can be used to anticipate the role of non-linear effects on the electron-phonon coupling, providing new insight into these barely studied effects. This paper is structured as follows. In Section II, we introduce electron-phonon coupling and show how it can be written in terms of electronic descriptors and derivatives of the electronic effective potential. In Section III, we propose four different real-space descriptors and analyze their magnitudes in a group of well-known conventional superconducting materials. The purpose of the analysis is twofold: (i) to assess the contribution of the derivatives of the potential to the electron-phonon coupling in hydrides, proposing a way of including those in a future model to predict T_c with more accuracy; and (ii) to evaluate the importance of non-linear effects of the potential in hydride superconductors. Finally, in Section IV we present a summary of the results and some conclusions.

II. ELECTRON-PHONON COUPLING

Under the Born-Oppenheimer (BO) approximation, ionic and electronic degrees of freedom are decoupled, and one can solve the system as two separate problems. Normally, the electronic Hamiltonian, \mathcal{H}_e , considers that the M nuclei and its inner cores are fixed in some ionic positions, $\mathbf{R} = \{\mathbf{R}_1, \dots, \mathbf{R}_M\}$, that are treated parametrically. In density functional theory, it is possible to find the one-electron wavefunctions,

$\psi_i(\mathbf{r}; \mathbf{R})$, by solving the Kohn-Sham (KS) equations,

$$\left[-\frac{1}{2} \nabla_{\mathbf{r}}^2 + v_{KS}(\mathbf{r}; \mathbf{R}) \right] \psi_i(\mathbf{r}; \mathbf{R}) = \varepsilon_i \psi_i(\mathbf{r}; \mathbf{R}), \quad (1)$$

where $v_{KS}(\mathbf{r}; \mathbf{R})$, the Kohn-Sham potential, is a one-body effective potential acting on the electrons. It contains the attractive ionic potential, the Coulomb repulsion between electrons, and an approximate term accounting for exchange and correlation.

In the case of a crystal, we consider a supercell containing N_c unit cells, satisfying periodic boundary conditions (PBCs), where eigenstates are the Bloch functions, $\psi_i(\mathbf{r}) = \psi_{n\mathbf{k}}(\mathbf{r}) = \langle \mathbf{r} | n\mathbf{k} \rangle$. The indices n, \mathbf{k} indicate both the band index and the momentum, respectively. When ions are perturbed out of their equilibrium positions, the KS potential felt by the electrons also fluctuates. It is thus possible to measure the coupling between the electrons and the phonons in a crystal by assessing the magnitude of those changes. In fact, the electron-phonon matrix elements depend on the derivatives of v_{KS} with respect to lattice distortions,

$$g_{m\mathbf{k}, n\mathbf{k}'}^a = \left\langle m\mathbf{k} \left| \frac{\partial v_{KS}(\mathbf{r}; \mathbf{R})}{\partial u_a} \right|_{u_a=0} \right| n\mathbf{k}' \rangle, \quad (2)$$

where u_a are the displacements of the ionic positions from equilibrium, and the subscript $a = (i\alpha)$ refers to the ionic site i in the supercell, and the Cartesian coordinate α . For simplicity, we consider distortions from equilibrium that have the periodicity of the supercell and are otherwise completely general, i.e. we do not consider monochromatic perturbations with finite wavevector \mathbf{q} , that would imply distortions not commensurate with the supercell. The electron-phonon coupling constant,

$$\lambda = 2 \int d\omega \frac{\alpha^2 F(\omega)}{\omega}, \quad (3)$$

is often used to assess the magnitude of the coupling, and depends directly on the matrix elements through the Eliashberg function,

$$\alpha^2 F(\omega) = \sum_{a,b} \Delta_{ab} B_{ab}(\omega), \quad (4)$$

where Δ_{ab} is the averaged deformation potential over the Fermi surface,

$$\Delta_{ab} = \frac{1}{N_F N_{\mathbf{k}}} \sum_{n, m, \mathbf{k}, \mathbf{k}'} g_{m\mathbf{k}, n\mathbf{k}'}^a g_{n\mathbf{k}', m\mathbf{k}}^b \times \delta(\varepsilon_{m\mathbf{k}} - \varepsilon_F) \delta(\varepsilon_{n\mathbf{k}'} - \varepsilon_F), \quad (5)$$

and $B_{ab}(\omega)$ is the phonon spectral function.[53, 54] In Eq. (5) N_F is the density of states per spin at the Fermi level and $N_{\mathbf{k}}$ the number of \mathbf{k} points in the sum.

III. REAL-SPACE DESCRIPTORS OF THE DERIVATIVES OF THE KS POTENTIAL

Equation (2) puts into evidence that the coupling between electrons and phonons depends on two things: the derivatives of the KS potential with respect to ionic displacements, and the overlap between the electronic states. The contribution of the former on the magnitude of electron-phonon coupling and critical temperature of hydrogen-based superconductors has not been studied before in the literature. After reviewing the electronic descriptors that allow to describe hydride superconductors, the aim of this section is to analyze, from first principles, the real-space derivatives of the KS potential and its relationship to the critical temperature of some well-known superhydrides.

A. Electronic descriptors

The utility of electronic real-space descriptors to characterize hydrogen-based superconductors has now been demonstrated many times, with the electron localization function (ELF) being particularly good at describing those materials. It is defined as

$$ELF(\mathbf{r}) = \left[1 + \left(\frac{\tau(\mathbf{r}) - \tau_{vW}(\mathbf{r})}{\tau_{TF}(\mathbf{r})} \right)^2 \right]^{-1}, \quad (6)$$

with $\tau(\mathbf{r})$ the kinetic energy density of the system, depending on the KS wavefunctions, while $\tau_{vW}(\mathbf{r})$ and $\tau_{TF}(\mathbf{r})$ are the von Weizsäcker and Thomas-Fermi approximations to it, which depend directly on the electron density [34, 35, 55].

The maxima of the ELF are located in regions where opposite-spin electrons are likely to be found, providing a quantitative way of assessing the types of bond present in the lattice, which in turn allows a categorization of hydrogen-rich compounds into different families. This permits to identify high- T_c compounds, which are usually either of covalent character, or present a clathrate-like structure with hydrogens weakly bonded to each other in elongated bonds [31]. The molecularity index (ϕ^*), defined as the highest ELF value for which two hydrogens connect within the same isosurface, automatizes the bond-type categorization and therefore the screening of promising compounds [32].

Perhaps the most useful electronic descriptor proposed so far is the networking value, ϕ , introduced by Belli *et al.* in Ref. 31, defined as the highest ELF isovalue that creates a fully connected isosurface that is periodic in three dimensions. This quantity measures the degree of electronic delocalization, and it shows a positive correlation with T_c , which can be improved by

including some extra ingredients: the fraction of hydrogen atoms in the unit cell, H_f , and the fraction of the density of states at the Fermi energy that projects onto hydrogen orbitals, H_{DOS} .

Several fits have been proposed to estimate T_c from those four descriptors (ϕ , ϕ^* , H_f , and H_{DOS}) [31, 32, 36]. In the following, we use the Gradient Boosting Regression (GBR) fit proposed in Ref. 36, as a reference for predictions of T_c that consider purely electronic information. This is done using TcESTIME, a program that automatically searches for the ELF-derived descriptors and consequently estimates T_c [36, 56].

All in all, the electronic descriptors have boosted a better understanding of what drives superconductivity in hydrides from a chemical point of view. The estimations of T_c are useful because of their simplicity, but they lack accuracy, with predictions showing mean absolute errors around 33K in T_c , and even rising to 100 K in a few problematic compounds.[36] This motivates the search for other descriptors that include the effect of the derivative of the KS potential due to ionic vibrations on the electron-phonon coupling.

B. Systems of study

In this work, we analyze the derivatives of the Kohn-Sham potential in real space in some well-known superconductors. Two compounds with high critical temperature but different chemical bonding are studied, namely the clathrate-like $Fm\bar{3}m$ -LaH₁₀ structure at 150 GPa, with calculated $T_c = 250$ K,[2, 41] and the covalent $Im\bar{3}m$ -H₃S structure at 150 and 200 GPa, with T_c 's of 225 K and 204 K, respectively, also theoretically estimated.[1, 40, 57] A similar covalent structure where sulfur is replaced by selenium is also included in the analysis, which is predicted to have a considerably lower critical temperature of 116 K at 200 GPa,[58] nearly half of that of the very similar H₃S. This is a case where the electronic descriptors fail to capture the differences between the two systems (see Table I), which share similar ELF patterns and have close networking values of 0.66 and 0.69 for H₃Se and H₃S, respectively. Palladium hydride is also included in the analysis, a compound without any covalent bonds and where Pd and H atoms remain isolated, for which $T_c = 5$ K according to theoretical predictions.[59] Finally, we include the aluminum crystal for comparison, a conventional superconductor that does not contain hydrogen atoms, and presents a T_c barely above 1 K [60]. The variety of this sample of superconductors should serve to properly examine the similarities and differences between the derivatives of the KS potentials, and eventually capture useful information that was missing in the electronic contribution

addressed previously. For this aim, in the following we define some real-space descriptors that will help us better analyze the derivatives of the KS potential.

C. Contribution to electron-phonon coupling

The derivatives of the Kohn-Sham potential present in the matrix elements $g_{m\mathbf{k},n\mathbf{k}'}$ of Eq. (2) are taken with respect to the displacement of one of the atoms in one of its coordinates, represented by the vector $\mathbf{u}_a = u_a \hat{\mathbf{u}}_a$, with u_a the magnitude of the displacement and $\hat{\mathbf{u}}_a$ a unitary vector in the given Cartesian direction. This is then repeated for the rest of the atoms and directions, resulting on a total of $3M$ derivatives that contribute to the electron-phonon coupling, as it can be seen in Eqs. (4) and (5). Thus, we define a real-space descriptor that sums the contribution of all of those derivatives,

$$D^2(\mathbf{r}) = \sum_a \left(\frac{\partial v_{KS}(\mathbf{r})}{\partial u_a} \right)_{u_a=0}^2, \quad (7)$$

where the square is taken in order to avoid cancellation of positive and negative terms. One can study the topology of $D^2(\mathbf{r})$ in the materials of interest by analyzing its isosurfaces and critical points in the same way that it was done with the ELF.

In Fig. 1, one can see that the maxima of $D^2(\mathbf{r})$ are located on the atomic sites, which is expected, as the profile of the potential is quite steep in that region and any ionic displacements greatly affect its immediate surroundings. In turn, the intermediate values are found along the bonding axes. This can be seen for H₃S and LaH₁₀, where the highest critical points of D^2 connecting the maxima are, respectively, along the H-S bond direction, and between the hydrogen atoms. In fact, the D^2 isosurfaces reveal a pattern of connections between nuclei in a similar way than the ELF did (see Fig. 1), showing that the types of chemical bonds present in the materials also affect the electron-phonon coupling through the derivatives. This explains the success of the classification of systems into families according to the dominant type of bond appearing in the lattice [31].

In the case of PdH, the topology of D^2 is again reminiscent of that of the ELF, as the critical points appear at very low isovalues ($0.94Ry^2/a_0^2$ compared to $4.8Ry^2/a_0^2$ for H₃S), showing the isolated nature of the bonds. Those lower values anticipate how in this system the contribution of the derivatives to the electron-phonon coupling should be lower, too. On the other hand, in the aluminum crystal the derivatives are low everywhere, even in the atomic cores, owing to the lack of hydrogen in the lattice. In contrast to the other compounds, the isosurfaces are very different from those

Table I: Summary of reference values and results for the different systems of study, including: pressure (P), networking value (ϕ), molecularity index (ϕ^*), DOS hydrogen fraction (H_{DOS}), hydrogen fraction (H_f), predicted T_c using electronic descriptors obtained with GBR fit of TcESTIME (T_c^{GBR}), and reference critical temperature obtained from the literature (T_c^{ref}), as well as the work from where those were taken.

	P (GPa)	ϕ	ϕ^*	H_{DOS}	H_f	T_c^{GBR} (K)	T_c^{ref} (K)	Ref.
Al	0	0.61	-	0.000	0.000	-	1.2	[60]
PdH	0	0.21	0.21	0.101	0.500	9	5	[59]
H ₃ Se	200	0.66	0.66	0.479	0.750	194	116	[58]
H ₃ S	200	0.69	0.69	0.473	0.750	201	204	[57]
H ₃ S	150	0.71	0.71	0.488	0.750	223	225	[40]
LaH ₁₀	150	0.56	0.67	0.591	0.909	253	250	[41]

of the ELF, which shows its metallic bond character, where electrons are delocalized throughout the lattice (see Fig. 1(b)). The analysis of $D^2(\mathbf{r})$, on the other hand, suggests that the effect of the vibrations on the electronic potential is quite local.

The results in aluminum and palladium hydride suggest that high localization of electrons in regions of large derivatives of v_{KS} could be beneficial for enhancing the electron-phonon coupling. While the derivatives are low in both cases, leading to low electron-phonon coupling, in Al the valence electrons are located in regions where the KS potential barely fluctuates, as it is evidenced by the mismatch between the ELF and $D^2(\mathbf{r})$, which could be the reason behind its lower T_c (see Table I).

In order to have a single value that measures the magnitude of the derivatives for each compound, we define

$$D^2 = \frac{1}{\Omega_v} \int_{\Omega_v} D^2(\mathbf{r}) d\mathbf{r}, \quad (8)$$

where the integral is taken over the valence volume, Ω_v , which considers the unit cell without the region of the cores, defined by the core radii presented in Table III. This is done because $D^2(\mathbf{r})$ is highly dependent on the pseudopotential, and only considering the valence region leads to more consistent results across different theoretical approaches (see Appendix B). The values of D^2 are presented in Table II for all the compounds studied in this paper. This magnitude is clearly larger in H₃S than in H₃Se, properly capturing the more pronounced electron-phonon coupling that leads to a higher T_c in the former. Like this, D^2 seizes what previous electronic-only-based T_c descriptors failed to capture.

Although better at distinguishing those two compounds, D^2 does not place the critical temperatures of the hydrides in a perfect growing order. However, this is compensated by the electronic descriptors previously described, i.e. ϕ , H_{DOS} , and H_f . In Figure 2 we present a combination of those with D^2 , and observe that the

correlation with the reference T_c is improved in comparison with what was obtained when predicting only with electronic descriptors, using T_c^{GBR} . In fact, in this database the mean absolute error of the prediction is reduced from 21 K to 15 K. The product $H_f\phi H_{DOS}D^2$, and the linear fit obtained from its correlation with T_c , is only intended to illustrate the power of D^2 to improve the characterization of high- T_c compounds, and it is not proposed as a new fit to estimate T_c , as the database is too small to justify a generalization. Nonetheless, the integral of $D^2(\mathbf{r})$ is a good candidate to add to the list of simple descriptors that can be used to fit the critical temperature, e.g. using machine learning. In order to have an improved model that does more accurate predictions, a larger database of hydrogen compounds would be needed.

Table II: Summary of results for the integrated descriptors proposed in this contribution, including D^2 , the absolute difference between σ_{KS}^2 and D^2u^2 , and ΔV_{KS} for the different systems of study.

	P (GPa)	D^2 (Ry^2/a_0^2)	$ \sigma_{KS}^2 - D^2u^2 $ (Ry^2)	ΔV_{KS} (Ry)
Al	0	0.52	0.000	0.003
PdH	0	0.49	0.014	0.014
H ₃ Se	200	1.57	0.007	0.023
H ₃ S	200	1.94	0.005	0.025
H ₃ S	150	1.82	0.005	0.023
LaH ₁₀	150	1.73	0.008	0.027

D. Beyond the linear approximation

The standard approach to assess the magnitude of electron-phonon coupling, both in superconductors as in other materials, is to estimate the matrix elements in Eq. (2) that contain the first derivative of the KS poten-

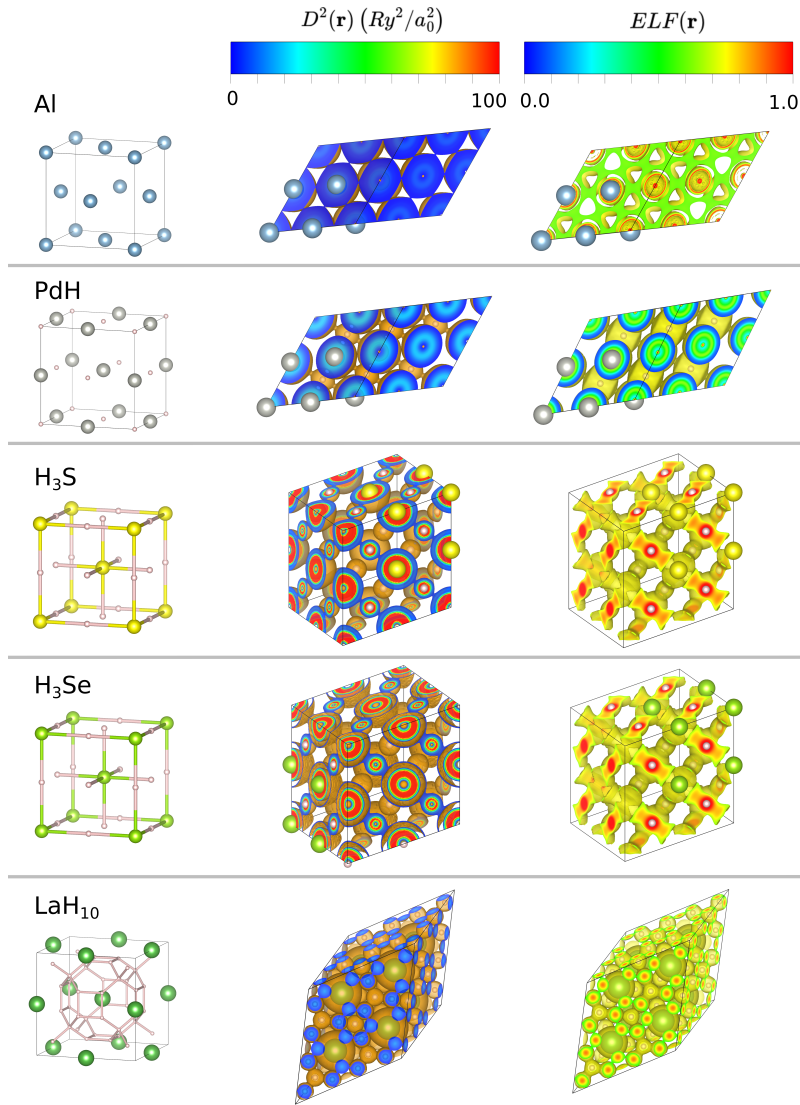


Figure 1: In the right pannel, structures of (a) Al, (b) PdH, (c) H₃S, (d) H₃Se, and (e) LaH₁₀. In the center, isosurfaces of D^2 at the critical point where all atoms get connected: Al at $D^2 = 0.38 Ry^2/a_0^2$, PdH at $D^2 = 0.94 Ry^2/a_0^2$, H₃S (150 GPa) at $D^2 = 4.8 Ry^2/a_0^2$, H₃Se at $D^2 = 3.8 Ry^2/a_0^2$, and LaH₁₀ at $D^2 = 2.2 Ry^2/a_0^2$. To the right, ELF isosurfaces of Al at 0.6, PdH at 0.21, H₃S at 0.7., H₃Se at 0.65, and LaH₁₀ at 0.56.

tial. This formulation is actually derived from a Taylor expansion of the potential when the system undergoes a perturbation from its equilibrium ionic positions,

$$v_{KS}(\mathbf{r}; \mathbf{R}^0 + \mathbf{u}) = v_{KS}(\mathbf{r}; \mathbf{R}^0) + \sum_a \left. \frac{\partial v_{KS}}{\partial u_a} \right|_{\mathbf{u}=0} u_a + \frac{1}{2} \sum_{a,b} \left. \frac{\partial^2 v_{KS}}{\partial u_a \partial u_b} \right|_{\mathbf{u}=0} u_a u_b + \dots \quad (9)$$

Then, the appearance of the first derivatives in the matrix elements stems from a linear approximation of the potential,

$$v_{KS}(\mathbf{r}; \mathbf{R}^0 + \mathbf{u}) - v_{KS}(\mathbf{r}; \mathbf{R}^0) \approx \sum_a \left. \frac{\partial v_{KS}}{\partial u_a} \right|_{\mathbf{u}=0} u_a. \quad (10)$$

To our knowledge, not much has been said about the validity and scope of the approximation made in Eq. (10). However, there are some reasons to believe

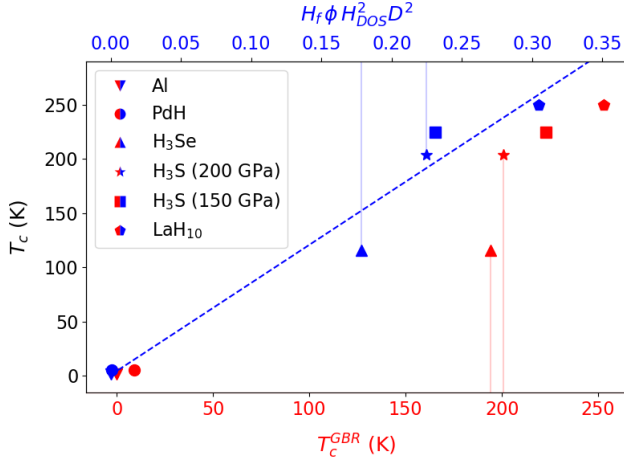


Figure 2: Comparison of the correlations between the reference critical temperature, T_c , with two different quantities. In red, it is contrasted with the predictions made with electronic descriptors, T_c^{GRR} . In blue, T_c is displayed against a new combination of descriptors including derivatives of the KS potential, $H_f \phi H_{DOS}^2 D^2$, with the dashed line representing a linear fit to predict the critical temperature from that quantity. Vertical lines highlight the ability of the second model to distinguish the different critical temperatures of H_3Se and H_3S at 200 GPa.

that it might be insufficient in hydrides. When one studies the phonon modes of those materials, a similar expansion is done on the Born-Oppenheimer potential upon lattice distortions. In hydrogen-based compounds, the contribution of higher-order derivatives has proven to be significant, and only taking lower-order derivatives leads to important errors in the determination of the phonon modes and the equilibrium geometry. Because in both cases the potentials are expanded with respect to ionic displacements, which can be large for a light atom like hydrogen, a similar result is expected for the KS potential.

In Ref. 47, electron-phonon coupling was studied from a non-perturbative approach. There, it was shown how a non-linear description of the coupling in palladium hydride, i.e. taking derivatives beyond first order, greatly affects the estimation of the electron-phonon coupling constant, λ , while the contrary is observed for a simple metal such as aluminum. It is thus interesting to find a simple way to study the deviations from linearity of the KS potential in different hydrides, and determine the utility of the linear approximation in those systems.

One way to include the changes of v_{KS} in a non-perturbative way is to take its average over an ensemble

of distorted configurations. We consider a Gaussian probabilistic ionic distribution $\varrho(\mathbf{R})$ centered at \mathcal{R} ,

$$\varrho(\mathbf{R}) = \frac{1}{\sqrt{\det(2\pi\Psi)}} \times \exp \left[-\frac{1}{2} \sum_{a,b} (R_a - \mathcal{R}_a) \Psi_{ab}^{-1} (R_b - \mathcal{R}_b) \right], \quad (11)$$

where Ψ is the displacement-displacement correlation matrix,

$$\Psi_{ab} = \langle u_a u_b \rangle = \frac{1}{\sqrt{M_a M_b}} \times \sum_{\mathbf{q}\nu} \frac{\hbar(2n_{\mathbf{q}\nu} + 1)}{2\omega_{\mathbf{q}\nu}} \eta_a(\mathbf{q}\nu) \eta_b(\mathbf{q}\nu), \quad (12)$$

with $\eta(\mathbf{q}\nu)$ the polarization vectors, $\omega_{\mathbf{q}\nu}$ the phonon frequencies, $n_{\mathbf{q}\nu}$ the Bose-Einstein occupation numbers and M_a, M_b the mass of the nuclei. In practice, we will take the distribution either from a harmonic approximation, or from the SSCHA, an approach that includes anharmonic effects while using an effective harmonic Hamiltonian (see Appendix A)[47].

Using the probability distribution in Eq. (11), we take the square of the two sides of Eq. (10), and average over an ensemble of perturbed configurations,

$$\int [v_{KS}(\mathbf{r}; \mathbf{R}^0 + \mathbf{u}) - v_{KS}(\mathbf{r}; \mathbf{R}^0)]^2 \varrho(\mathbf{u}) d\mathbf{u} = \int \sum_{a,b} \left. \frac{\partial v_{KS}}{\partial u_a} \right|_{u_a=0} \left. \frac{\partial v_{KS}}{\partial u_b} \right|_{u_b=0} u_a u_b \varrho(\mathbf{u}) d\mathbf{u}, \quad (13)$$

$$= \sum_a \left(\left. \frac{\partial v_{KS}}{\partial u_a} \right|_{u_a=0} \right)^2 \langle u_a^2 \rangle_{\varrho}. \quad (14)$$

Here, $\langle u_a^2 \rangle_{\varrho}$ is the root mean squared displacement, and it can be obtained from taking the diagonal of the displacement-displacement correlation matrix, Ψ_{aa} . Both sides of Eq. (14) are real-space functions that can be computed in the compounds studied in this work. For a perfectly linear system, both sides of the equation will be equal. We expect them to evidence larger differences in systems with a higher degree of non-linearity in the electron-phonon coupling.

The right hand side of Eq. (14),

$$(D^2 u^2)(\mathbf{r}) \equiv \sum_a \left(\left. \frac{\partial v_{KS}(\mathbf{r})}{\partial u_a} \right|_{u_a=0} \right)^2 \langle u_a^2 \rangle_{\varrho}, \quad (15)$$

is very similar to $D^2(\mathbf{r})$ and can be obtained in an analogous way. The only difference is that the derivatives are weighted by the root mean squared displacements of the atoms. Computing the left hand side of (14) requires a different approach, and in practice the integral is approximated by an explicit average over a finite number of N_c distorted configurations (see Appendix A),

$$\begin{aligned} \sigma_{KS}^2(\mathbf{r}) &\equiv \int [v_{KS}(\mathbf{r}; \mathbf{R}^0 + \mathbf{u}) - v_{KS}(\mathbf{r}; \mathbf{R}^0)]^2 \varrho(\mathbf{u}) d\mathbf{u}, \\ &\approx \frac{1}{N_c} \sum_{I=1}^{N_c} [v_{KS}(\mathbf{R}^0 + \mathbf{u}_I) - v_{KS}(\mathbf{R}^0)]^2, \end{aligned} \quad (16)$$

where \mathbf{u}_I is the displacement from equilibrium of the I -th perturbed configuration, obtained according to the probability distribution, $\varrho(\mathbf{u})$. The approximation becomes exact at the limit $N_c \rightarrow \infty$.

Computing $(D^2u^2)(\mathbf{r})$ and $\sigma_{KS}^2(\mathbf{r})$ on the same compounds as before, we notice that, at first glance, the real-space isosurfaces of Eqs. (15) and (16) do not provide much information about the magnitude of the non-linear terms in the systems of study (see Appendix C). Thus, we again integrate the valence regions of the supercell to define the global quantities,

$$D^2u^2 = \frac{1}{\Omega_v} \int_{\Omega_v} (D^2u^2)(\mathbf{r}) d\mathbf{r}, \quad (17)$$

$$\sigma_{KS}^2 = \frac{1}{\Omega_v} \int_{\Omega_v} \sigma_{KS}^2(\mathbf{r}) d\mathbf{r}. \quad (18)$$

As it can be seen in Table II, the results show how the aluminum crystal stands out as the compound where the linear approximation is most adequate, in comparison with all the other hydrogen-based superconductors. Indeed, we observe that the integrals D^2u^2 and σ_{KS}^2 are almost equal in Al, while in the other systems their difference is an order of magnitude larger.

Another way of assessing non-linearity can be obtained if one does not take the square before integrating in Eq. (14), obtaining a quantity that is formally zero, due to the parity of the gaussian probability distribution,

$$\begin{aligned} \Delta v_{KS}(\mathbf{r}) &\equiv \int [v_{KS}(\mathbf{r}; \mathbf{R}^0 + \mathbf{u}) - v_{KS}(\mathbf{r}; \mathbf{R}^0)] \varrho(\mathbf{u}) d\mathbf{u} \\ &= 0. \end{aligned} \quad (19)$$

$$= \int \sum_a \frac{\partial v_{KS}}{\partial u_a} \Big|_{u=0} u_a \varrho(\mathbf{u}) d\mathbf{u} = 0. \quad (20)$$

Then, the global descriptor

$$\Delta V_{KS} = \frac{1}{\Omega_v} \int_{\Omega_v} |\Delta v_{KS}(\mathbf{r})| d\mathbf{r}, \quad (21)$$

will only be different from zero when there is a deviation from the linear regime. Here, the absolute value was considered in order to avoid cancelation of positive and negative terms. The results are collected in Table II.

The non-linear effects measured by ΔV_{KS} are easier to visualize, and again we see that the systems containing hydrogen show deviations from linearity an order of magnitude larger than that of aluminum. In particular, the results obtained for aluminum and palladium hydride are in agreement with previous observations, as the former is known to have a linear behavior, whereas in the latter this approximation has proved to be insufficient [47]. We are not aware of any previous studies on the importance of the non-linear terms of the KS potential for other hydrides. The descriptors proposed in this work predict that indeed the non-linear effects will be important across all the hydrides here presented. This will impact important quantities depending on electron-phonon matrix elements such as the Eliashberg function, coupling constant, and critical temperature. It thus becomes essential to continue to develop new methods that allow the inclusion of non-linear effects and more accurately represent the underlying physics.

IV. CONCLUSIONS

In this work, we studied the changes of the KS potential under ionic perturbations from equilibrium, and analyzed their effect on the electron-phonon coupling. This was done with two different aims: to assess the importance of the derivatives of v_{KS} on the estimation of the electron-phonon coupling constant and consequently on T_c ; and to understand the limitations of approximating the KS potential linearly with respect to those changes. In both cases, real-space local and global quantities were proposed and later evaluated on well-known superconductors, considering compounds with and without hydrogen.

The spatial representation of the derivatives of v_{KS} obtained with $D^2(\mathbf{r})$ in hydrogen-based compounds showcased a qualitative correlation between the regions of higher variations of the potential and those of higher electron localization, as determined by the ELF. This analysis further supports the classification of materials according to their bonding type first presented in Ref. 31, which serves as a tool to recognize promising structures with higher critical temperatures. The correlation between those spatial patterns explains the success of the descriptors stemming from the ELF to predict the critical temperatures. Nonetheless, the information contained in the derivatives of the potential is necessary to construct a more complete picture of electron-phonon coupling. In fact, in the case of Al,

both functions display completely different shapes and, while the high electron delocalization is a signature of the metallic character of the system, the fluctuations of the KS potential far from the cores are not as important, which results in weak coupling. Indeed, a problem with the ELF-derived descriptors is that it could create *false positives* when there is a good metal, which is not necessarily conducive to a high T_c . In turn, the derivatives of v_{KS} can help properly classify such cases. Similarly, the integral of the local descriptor quantifies the magnitude of the derivatives in all of the valence region, which allows to properly describe the differences in the electron-phonon coupling in systems with similar bonding patterns. Such is the case of H_3S and H_3Se in the $Im\bar{3}m$ phase, which have coincident ELFs but show larger differences in the derivatives of the potential, explaining the large discrepancy between their critical temperatures. The proposed descriptor is thus a good candidate to join other quantities used in the fast first estimations of T_c in superhydrides.

The assessment of the fitness of the linear approximation in the study of electron-phonon coupling showed that the approach is insufficient to fully describe the phenomenon in hydride superconductors. This demonstrates the non-linearity of the potential in those materials, as it had been previously discussed for the case of palladium hydride [47]. Our method predicts H_3S , H_3Se , and LaH_{10} to be non-linear, too, meaning that care must be taken when λ is computed in the standard (linear) approach, as it might not be as exact as expected. Ideally, as it is done in Ref. 47 for Al and PdH, higher order derivatives should be performed to obtain more accurate results. Alternatively, the simplicity of the statistically averaged descriptors proposed in this contribution can serve as a practical tool to diagnose the degree of non-linearity of the potential in the system.

ACKNOWLEDGMENTS

This work is supported by the European Research Council (ERC) under the European Unions Horizon 2020 research and innovation program (Grant Agreement No. 802533 and 810367), the Spanish Ministry of Science and Innovation (Grant No. PID2022142861NA-I00), the Department of Education, Universities and Research of the Eusko Jauriaritza and the University of the Basque Country UPV/EHU (Grant No. IT1527-22), IKUR strategy—an initiative of Department of Science, Universities and Innovation of the Basque Government, and Simons Foundation through the Collaboration on New Frontiers in Superconductivity (Grant No. SFI-MPS-NFS-00006741-10). The authors also

thank ANR TcPredictor S22-ERC036, ANR Fiscency S23-JRAR060, EMERGENCE-SU H20X S23JR31014, GENCI A0040710377 for funding and resources.

Appendix A: Methods

The Kohn-Sham potentials used throughout this work, as well as the ELF and the DOS, are obtained during post-processing of a self-consistent field (SCF) calculation performed using the Quantum ESPRESSO plane-wave package.[61, 62] The estimated critical temperature, T_c^{GRR} , was obtained using TcESTIME.[36] For each material, a 2x2x2 supercell was used in order to properly describe the effect of phonon fluctuations. The lattice parameters and atomic positions of PdH, H_3S at 150 GPa, and LaH_{10} have been taken from the literature [40, 41, 59]. For H_3Se and H_3S at 200 GPa, the initial structure was taken from the literature, [57, 58] but were later relaxed, obtaining the lattice constants $a = 3.153 \text{ \AA}$ and $a = 2.988 \text{ \AA}$ for the unit cell, respectively. The fcc aluminum crystal was also relaxed, obtaining a unit cell lattice constant of $a = 2.021 \text{ \AA}$. DFT calculations are done within generalized-gradient approximation, using the PBE exchange-correlation functional [63]. Plane-augmented wave (PAW) pseudopotentials are employed for all the elements, considering only the local component of the KS potential in the analysis. For each system, a Methfessel–Paxton smearing of 0.02 Ry was used, whereas the energy cutoff for the wavefunctions and density were converged. Those were set to 70 Ry and 700 Ry, respectively, for H_3S and PdH. For Al, those values were set to 40 Ry and 400 Ry, to 50 Ry and 500 Ry for LaH_{10} , and to 60 Ry and 600 Ry for H_3Se . The k-points were sampled using a uniform Monkhorst-Pack grid, which was also converged for each compound. A grid of size 18x18x18 was used for Al, of 10x10x10 for PdH, 26x26x26 for H_3Se , 22x22x22 for H_3S at 200 GPa, 16x16x16 for H_3S at 150 GPa, and 6x6x6 for LaH_{10} .

Phonon calculations were performed on all systems, in order to obtain the dynamical matrices needed in the computation of the ionic probability distribution, $\rho(\mathbf{u})$, and the root mean squared displacements. In the case of PdH, LaH_{10} , and H_3S at 150 GPa, this was done at the stochastic self-consistent harmonic approximation (SSCHA) level, with the details of the calculations being the same as in Refs. [40, 41, 59]. For Al, H_3Se , and H_3S at 200 GPa, the harmonic approximation was employed, using density functional perturbation theory as implemented in Quantum ESPRESSO.

The derivatives of the KS potential are obtained using

finite differences,

$$\left. \frac{\partial v_{KS}(\mathbf{r}; \mathbf{R}^0 + u_a)}{\partial u_a} \right|_{u_a=0} \approx \frac{v_{KS}(\mathbf{r}; \mathbf{R}^0 + \mathbf{u}_a) - v_{KS}(\mathbf{r}; \mathbf{R}^0)}{u_a}, \quad (\text{A1})$$

taking $\mathbf{u}_a = u_a \hat{\mathbf{u}}_a$ as a vector of length $u_a = 0.01 \text{ \AA}$ displacing the i -th ion in the cartesian direction α , where $a = (i, \alpha)$. The resulting derivatives are summed to get $D^2(\mathbf{r})$. A similar thing is done for $D^2 u^2(\mathbf{r})$, but in that case the root mean squared displacement is also needed, $\langle u_a^2 \rangle$. It is obtained through Eq. (12) and computed using the CellConstructor package of the SSCHA Python-API.[45]

As it was previously mentioned, the statistical averages needed to compute $\sigma_{KS}^2(\mathbf{r})$ and $\Delta v_{KS}(\mathbf{r})$ are done in an approximate fashion, using a number of N_c perturbed configurations (see Eq. (16)). The distorted positions are obtained from the probability distribution $\varrho(\mathbf{u})$, also computed with the CellConstructor package. To accelerate convergence with respect to N_c , we increase the number of configurations by using the symmetry operations of the crystal. Then, if \mathbf{S} is one of those symmetry operations, and $v_{KS}(\mathbf{r}, \mathbf{R}_I)$ is known, with $\mathbf{R}_I = \mathbf{R}^0 + \mathbf{u}_I$, we can rotate the grid of points \mathbf{r} to obtain

$$v_{KS}(\mathbf{r}; \mathbf{S}\mathbf{R}_I) = v_{KS}(\mathbf{S}^{-1}\mathbf{r}; \mathbf{R}_I), \quad (\text{A2})$$

In this way, we have access to the KS potential for a perturbed configuration with ionic positions $\mathbf{S}\mathbf{R}_I$, without the need of doing a SCF calculation. Like this, we can include in Eq. (16) as many perturbed configurations per DFT calculation as the number of symmetry operations of the crystal, N_{symm} . For each system, 50 distinct distorted configurations, leading to a total of $N_c = 50N_{symm}$ terms in the sum in the estimation of $\sigma_{KS}^2(\mathbf{r})$ and $\Delta v_{KS}(\mathbf{r})$, were considered.

Appendix B: Core radii

In Table III we specify the radii used for the integration of the core. As shown in Fig. 3, once the core has been removed from the integration the result becomes independent of the pseudopotential used.

Appendix C: Isosurfaces of other descriptors

In Fig. 4 we show isosurfaces of $D^2 u^2(\mathbf{r})$ and $\sigma_{KS}^2(\mathbf{r})$ for comparison.

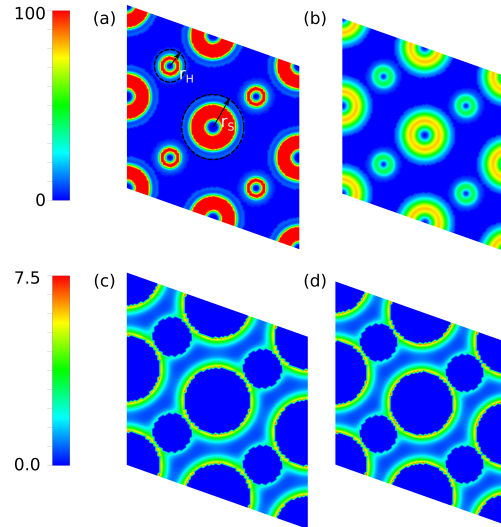


Figure 3: Comparison of $D^2(\mathbf{r})$ values along a plane in the H_3S crystal at 200 GPa, inside and outside the cores, defined by the radius $r_S = 1.7 a_0$ for sulfur and $r_H = 1.0 a_0$ for hydrogen, as depicted in (a). On the top panel, the colormap shows the values inside the core when using (a) plane augmented wave and (b) norm-conserving pseudopotentials. Using the same pseudopotentials, the values of $D^2(\mathbf{r})$ outside the cores are depicted in (c) and (d), respectively.

Element	$r_c(a_0)$
H	1.0
Al	1.9
S	1.7
Se	1.9
Pd	2.6
La	2.0

Table III: Cutoff radius, r_c , used in the integration of D^2 and other real-space quantities. It corresponds to the radius used for the generation of the ultrasoft pseudopotentials found in Quantum ESPRESSO, which is the largest radius compared to those used in other kinds of pseudopotential.

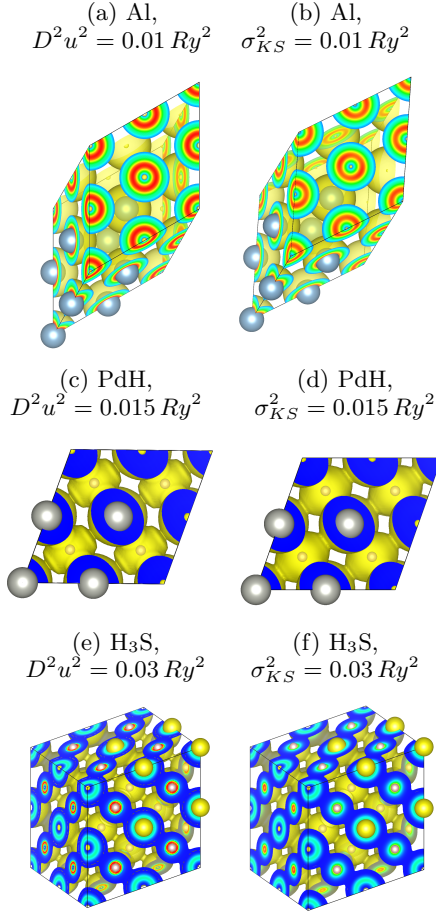


Figure 4: Comparison between isosurfaces of $D^2u^2(\mathbf{r})$ and $\sigma_{KS}^2(\mathbf{r})$ in Al, PdH and H3S at 150 GPa.

-
- [1] A. P. Drozdov, M. I. Erements, I. A. Troyan, V. Ksenofontov, and S. I. Shylin, Conventional superconductivity at 203 kelvin at high pressures in the sulfur hydride system, *Nature* **525**, 73 (2015).
- [2] A. Drozdov, P. Kong, V. Minkov, S. Besedin, M. Kuzovnikov, S. Mozaffari, L. Balicas, F. Balakirev, D. Graf, V. Prakapenka, *et al.*, Superconductivity at 250 k in lanthanum hydride under high pressures, *Nature* **569**, 528 (2019).
- [3] P. Kong, V. S. Minkov, M. A. Kuzovnikov, A. P. Drozdov, S. P. Besedin, S. Mozaffari, L. Balicas, F. F. Balakirev, V. B. Prakapenka, E. Greenberg, and M. I. Erements, Superconductivity up to 243 k in yttrium hydrides under high pressure, *Nature Communications* **12**, <https://doi.org/10.1038/s41467-021-25372-2> (2021).
- [4] W. Chen, D. V. Semenok, X. Huang, H. Shu, X. Li, D. Duan, T. Cui, and A. R. Oganov, High-temperature superconducting phases in cerium superhydride with a t c up to 115 k below a pressure of 1 megabar, *Physical Review Letters* **127**, 117001 (2021).
- [5] D. V. Semenok, I. A. Troyan, A. G. Ivanova, A. G. Kvashnin, I. A. Kruglov, M. Hanfland, A. V. Sadakov, O. A. Sobolevskiy, K. S. Pervakov, I. S. Lyubutin, K. V. Glazyrin, N. Giordano, D. N. Karimov, A. L. Vasiliev, R. Akashi, V. M. Pudalov, and A. R. Oganov, Superconductivity at 253 k in lanthanum–yttrium ternary hydrides, *Materials Today* **48**, 18 (2021).
- [6] J. Bi, Y. Nakamoto, P. Zhang, K. Shimizu, B. Zou, H. Liu, M. Zhou, G. Liu, H. Wang, and Y. Ma, Giant enhancement of superconducting critical temperature in substitutional alloy (la, ce) h9, *Nature Communications* **13**, 5952 (2022).
- [7] Z. Li, X. He, C. Zhang, X. Wang, S. Zhang, Y. Jia, S. Feng, K. Lu, J. Zhao, J. Zhang, *et al.*, Superconductivity above 200 k discovered in superhydrides of calcium, *Nature communications* **13**, 2863 (2022).

- [8] Y. Song, J. Bi, Y. Nakamoto, K. Shimizu, H. Liu, B. Zou, G. Liu, H. Wang, and Y. Ma, Stoichiometric ternary superhydride LaH_8 as a new template for high-temperature superconductivity at 110 K under 80 GPa, *Physical Review Letters* **130**, 266001 (2023).
- [9] S. Saha, S. Di Cataldo, F. Giannessi, A. Cucciari, W. von der Linden, and L. Boeri, Mapping superconductivity in high-pressure hydrides: The superhydride project, *Phys. Rev. Mater.* **7**, 054806 (2023).
- [10] W. Chen, X. Huang, D. V. Semenov, S. Chen, D. Zhou, K. Zhang, A. R. Oganov, and T. Cui, Enhancement of superconducting properties in the La-Ce-H system at moderate pressures, *Nature Communications* **14**, 2660 (2023).
- [11] U. Pinsook, P. Tsuppayakorn-Aek, and T. Bovornratanaarak, Superconductivity in hexagonal $\text{Ce}_{0.5}\text{La}_{0.5}\text{H}_9$ under high pressure, *Physical Chemistry Chemical Physics* **27**, 768 (2025).
- [12] K. Gao, T. F. Cerqueira, A. Sanna, Y.-W. Fang, Đ. Dangić, I. Errea, H.-C. Wang, S. Botti, and M. A. Marques, The maximum T_c of conventional superconductors at ambient pressure, *arXiv preprint arXiv:2502.18281* (2025).
- [13] Đ. Dangić, Y.-W. Fang, T. F. Cerqueira, A. Sanna, M. A. Marques, and I. Errea, Ambient pressure high temperature superconductivity in RbPH_3 facilitated by ionic anharmonicity, *arXiv preprint arXiv:2411.03822* (2024).
- [14] A. Sanna, T. F. Cerqueira, Y.-W. Fang, I. Errea, A. Ludwig, and M. A. Marques, Prediction of ambient pressure conventional superconductivity above 80 K in hydride compounds, *npj Computational Materials* **10**, 44 (2024).
- [15] T. F. T. Cerqueira, Y.-W. Fang, I. Errea, A. Sanna, and M. A. L. Marques, Searching materials space for hydride superconductors at ambient pressure, *Advanced Functional Materials* **34**, 2404043 (2024).
- [16] K. Dolui, L. J. Conway, C. Heil, T. A. Strobel, R. P. Prasankumar, and C. J. Pickard, Feasible route to high-temperature ambient-pressure hydride superconductivity, *Phys. Rev. Lett.* **132**, 166001 (2024).
- [17] J. A. Flores-Livas, L. Boeri, A. Sanna, G. Profeta, R. Arita, and M. Eremets, A perspective on conventional high-temperature superconductors at high pressure: Methods and materials, *Physics Reports* **856**, 1 (2020).
- [18] C. J. Pickard, I. Errea, and M. I. Eremets, Superconducting hydrides under pressure, *Annual Review of Condensed Matter Physics* **11**, 57 (2020).
- [19] M. J. Hutcheon, A. M. Shipley, and R. J. Needs, Predicting novel superconducting hydrides using machine learning approaches, *Phys. Rev. B* **101**, 144505 (2020).
- [20] K. P. Hilleke and E. Zurek, Tuning chemical precompression: Theoretical design and crystal chemistry of novel hydrides in the quest for warm and light superconductivity at ambient pressures, *Journal of Applied Physics* **131** (2022).
- [21] X. Wei, X. Hao, A. Bergara, E. Zurek, X. Liang, L. Wang, X. Song, P. Li, L. Wang, G. Gao, *et al.*, Designing ternary superconducting hydrides with a 15-type structure at moderate pressures, *Materials Today Physics* **34**, 101086 (2023).
- [22] S. Di Cataldo and L. Boeri, Metal borohydrides as ambient-pressure high- T_c superconductors, *Physical Review B* **107**, L060501 (2023).
- [23] Y.-W. Fang, Đ. Dangić, and I. Errea, Assessing the feasibility of near-ambient conditions superconductivity in the Lu-Ni-H system, *Communications Materials* **5**, 61 (2024).
- [24] F. Zheng, Z. Zhang, Z. Wu, S. Wu, Q. Lin, R. Wang, Y. Fang, C.-Z. Wang, V. Antropov, Y. Sun, *et al.*, Prediction of ambient pressure superconductivity in cubic ternary hydrides with MH_6 octahedra, *Materials Today Physics* **42**, 101374 (2024).
- [25] A. B. Migdal, Interactions between electrons and lattice vibrations in a normal metal, *Sov. Phys. - JETP (Engl. Transl.)* **34** (1958).
- [26] G. M. Eliashberg, Interactions between electrons and lattice vibrations in a superconductor, *Sov. Phys. - JETP (Engl. Transl.)* **11** (1960).
- [27] F. Marsiglio, Eliashberg theory: A short review, *Annals of Physics* **417**, 168102 (2020).
- [28] V. Stanev, C. Oses, A. G. Kusne, E. Rodriguez, J. Paglione, S. Curtarolo, and I. Takeuchi, Machine learning modeling of superconducting critical temperature, *npj Computational Materials* **4**, 29 (2018).
- [29] T. F. T. Cerqueira, A. Sanna, and M. A. L. Marques, Sampling the materials space for conventional superconducting compounds, *Advanced Materials* **36**, 2307085 (2024).
- [30] S. Xie, Y. Quan, A. Hire, B. Deng, J. DeStefano, I. Salinas, U. Shah, L. Fanfarillo, J. Lim, J. Kim, *et al.*, Machine learning of superconducting critical temperature from Eliashberg theory, *npj Computational Materials* **8**, 14 (2022).
- [31] F. Belli, T. Novoa, J. Contreras-García, and I. Errea, Strong correlation between electronic bonding network and critical temperature in hydrogen-based superconductors, *Nature Communications* **12**, 1 (2021).
- [32] M. E. Di Mauro, B. Braida, I. Errea, T. Novoa, and J. Contreras-García, Molecularly: A fast and efficient criterion for probing superconductivity, *Physical Review B* **110**, 174515 (2024).
- [33] W. A. Muriel, T. Novoa, C. Cárdenas, and J. Contreras-García, Introducing electron correlation in solid-state calculations for superconducting states, *Faraday discussions* **254**, 598 (2024).
- [34] K. E. Becke, A. D. and Edgecombe, A simple measure of electron localization in atomic and molecular systems, *J. Chem. Phys.* **92**, 5397 (1990).
- [35] A. Savin, R. Nesper, S. Wengert, and T. F. Fässler, Elf: The electron localization function, *Angew. Chem. Int. Ed. Engl.* **36**, 1808 (1997).
- [36] T. Novoa, M. E. di Mauro, D. Inostroza, K. El Haloui, N. Sisourat, Y. Maday, and J. Contreras-García, TcEstimate: predicting high-temperature hydrogen-based superconductors, *Chemical Science* (2024).

- [37] X. Li, X. Zhang, Y. Liu, and G. Yang, Bonding-unsaturation-dependent superconductivity in P-rich sulfides, *Matter and Radiation at Extremes* **7**, 048402 (2022).
- [38] R. H. Lavroff, J. Munarriz, C. E. Dickerson, F. Munoz, and A. N. Alexandrova, Chemical bonding dictates drastic critical temperature difference in two seemingly identical superconductors, *Proceedings of the National Academy of Sciences* **121**, e2316101121 (2024).
- [39] J. Yu, C. J. Ciccarino, R. Bianco, I. Errea, P. Narang, and B. A. Bernevig, Non-trivial quantum geometry and the strength of electron-phonon coupling, *Nature Physics*, 1 (2024).
- [40] I. Errea, M. Calandra, C. J. Pickard, J. R. Nelson, R. J. Needs, Y. Li, H. Liu, Y. Zhang, Y. Ma, and F. Mauri, Quantum hydrogen-bond symmetrization in the superconducting hydrogen sulfide system, *Nature* **532**, 81 (2016).
- [41] I. Errea, F. Belli, L. Monacelli, A. Sanna, T. Koretsune, T. Tadano, R. Bianco, M. Calandra, R. Arita, F. Mauri, *et al.*, Quantum crystal structure in the 250-kelvin superconducting lanthanum hydride, *Nature* **578**, 66 (2020).
- [42] P. Hou, F. Belli, R. Bianco, and I. Errea, Quantum anharmonic enhancement of superconductivity in p63/mmc sch6 at high pressures: a first-principles study, *Journal of Applied Physics* **130** (2021).
- [43] F. Belli and I. Errea, Impact of ionic quantum fluctuations on the thermodynamic stability and superconductivity of labh 8, *Physical Review B* **106**, 134509 (2022).
- [44] I. Errea, M. Calandra, and F. Mauri, Anharmonic free energies and phonon dispersions from the stochastic self-consistent harmonic approximation: Application to platinum and palladium hydrides, *Physical Review B* **89**, 064302 (2014).
- [45] L. Monacelli, R. Bianco, M. Cherubini, M. Calandra, I. Errea, and F. Mauri, The stochastic self-consistent harmonic approximation: calculating vibrational properties of materials with full quantum and anharmonic effects, *Journal of Physics: Condensed Matter* **33**, 363001 (2021).
- [46] R. Heid, Relevance of quadratic electron-phonon coupling for the superconducting transition temperature, *Physical Review B* **45**, 5052 (1992).
- [47] R. Bianco and I. Errea, Non-perturbative theory of the electron-phonon coupling and its first-principles implementation, *arXiv preprint arXiv:2303.02621* (2023).
- [48] H. Liu, Y. Yuan, D. Liu, X.-Z. Li, and J. Shi, Superconducting transition temperatures of metallic liquids, *Phys. Rev. Res.* **2**, 013340 (2020).
- [49] H. Chen, X.-W. Zhang, X.-Z. Li, and J. Shi, First-principles estimation of the superconducting transition temperature of a metallic hydrogen liquid, *Phys. Rev. B* **104**, 184516 (2021).
- [50] H. Chen and J. Shi, Stochastic path-integral approach for predicting the superconducting temperatures of anharmonic solids, *Phys. Rev. B* **106**, 184501 (2022).
- [51] X.-W. Zhang, H. Chen, E.-G. Wang, J. Shi, and X.-Z. Li, Nonperturbative *abinitio* approach for calculating the electrical conductivity of a liquid metal, *Phys. Rev. B* **105**, 155148 (2022).
- [52] H. Chen and J. Shi, Coexistence of superconductivity and superionicity in $\text{li}_2\text{mg}_2\text{h}_6$, *Phys. Rev. B* **109**, L140505 (2024).
- [53] P. B. Allen and B. Mitrović, Theory of superconducting tc, *Solid state physics* **37**, 1 (1983).
- [54] D. Dangić, L. Monacelli, R. Bianco, F. Mauri, and I. Errea, Large impact of phonon lineshapes on the superconductivity of solid hydrogen, *Communications Physics* **7**, 150 (2024).
- [55] Á. M. Pendás and J. Contreras-García, *Topological Approaches to the Chemical Bond* (Springer Nature, 2023).
- [56] TcESTIME code:
<https://github.com/juliaccontrerasgarcia/Tcetime>;
 TcESTIMEweb server: <https://lct-webtools.sorbonne-universite.fr/tcetime/>.
- [57] D. Duan, Y. Liu, F. Tian, D. Li, X. Huang, Z. Zhao, H. Yu, B. Liu, W. Tian, and T. Cui, Pressure-induced metallization of dense (h2s) 2h2 with high-t c superconductivity, *Scientific reports* **4**, 6968 (2014).
- [58] S. Zhang, Y. Wang, J. Zhang, H. Liu, X. Zhong, H.-F. Song, G. Yang, L. Zhang, and Y. Ma, Phase diagram and high-temperature superconductivity of compressed selenium hydrides, *Scientific reports* **5**, 15433 (2015).
- [59] I. Errea, M. Calandra, and F. Mauri, First-principles theory of anharmonicity and the inverse isotope effect in superconducting palladium-hydride compounds, *Phys. Rev. Lett.* **111**, 177002 (2013).
- [60] J. F. Cochran and D. E. Mapother, Superconducting transition in aluminum, *Phys. Rev.* **111**, 132 (1958).
- [61] P. Giannozzi, S. Baroni, N. Bonini, M. Calandra, R. Car, C. Cavazzoni, D. Ceresoli, G. L. Chiarotti, M. Cococcioni, I. Dabo, A. D. Corso, S. Fabris, G. Fratesi, S. de Gironcoli, R. Gebauer, U. Gerstmann, C. Gougoussis, A. Kokalj, M. Lazzeri, L. Martin-Samos, N. Marzari, F. Mauri, R. Mazzarello, S. Paolini, A. Pasquarello, L. Paulatto, C. Sbraccia, S. Scandolo, G. Sclauzero, A. P. Seitsonen, A. Smogunov, P. Umari, and R. M. Wentzcovitch, Quantum espresso: a modular and open-source software project for quantum simulations of materials, *J. Phys.: Condens. Matter* **21**, 395502 (2009).
- [62] P. Giannozzi, O. Andreussi, T. Brumme, O. Bunau, M. B. Nardelli, M. Calandra, R. Car, C. Cavazzoni, D. Ceresoli, M. Cococcioni, N. Colonna, I. Carnimeo, A. D. Corso, S. de Gironcoli, P. Delugas, R. A. D. Jr, A. Ferretti, A. Floris, G. Fratesi, G. Fugallo, R. Gebauer, U. Gerstmann, F. Giustino, T. Gorni, J. Jia, M. Kawamura, H.-Y. Ko, A. Kokalj, E. Küçükbenli, M. Lazzeri, M. Marsili, N. Marzari, F. Mauri, N. L. Nguyen, H.-V. Nguyen, A. O. de-la Roza, L. Paulatto, S. Poncé, D. Rocca, R. Sabatini, B. Santra, M. Schlipf, A. P. Seitsonen, A. Smogunov, I. Timrov, T. Thonhauser, P. Umari, N. Vast, X. Wu, and S. Baroni, Advanced capabilities for materials modelling with quantum espresso, *J. Phys.: Condens. Matter* **29**, 465901 (2017).

- [63] J. P. Perdew, K. Burke, and M. Ernzerhof, Generalized gradient approximation made simple, *Phys. Rev. Lett.* **77**, 3865 (1996).